

Role of spin-orbit coupling on the electronic structure and properties of SrPtAs

S. J. Youn^{1,2}, S. H. Rhim², D. F. Agterberg³, M. Weinert³, A. J. Freeman²

¹ Department of Physics Education and Research Institute of Natural Science,
Gyeongsang National University, Jinju 660-701, Korea

² Department of Physics and Astronomy, Northwestern University, Evanston, Illinois, 60208-3112, USA and

³ Department of Physics, University of Wisconsin-Milwaukee, Milwaukee, WI 53201-0413, USA

(Dated: February 9, 2012)

The effect of spin-orbit coupling on the electronic structure of the layered iron-free pnictide superconductor, SrPtAs, has been studied using the full potential linearized augmented plane wave method. The anisotropy in Fermi velocity, conductivity and plasma frequency stemming from the layered structure are found to be enhanced by spin-orbit coupling. The relationship between spin-orbit interaction and the lack of two-dimensional inversion in the PtAs layers is analyzed within a tight-binding Hamiltonian based on the first-principles calculations. Finally, the band structure suggests that electron doping could increase T_c .

PACS numbers: 74.20.Pq, 74.70.Xa, 71.20.-b, 71.18.+y

I. INTRODUCTION

The recent discovery of superconductivity in pnictides has attracted extensive attention owing to their surprisingly high T_c .¹ While the highest T_c so far is 56 K for GdFeAsO,² a consensus on the pairing mechanism has not yet been reached.³ This class of materials share a common crystal structure, that is, the Fe square lattice. While most of the superconducting pnictides are Fe-based, pnictides without iron also exhibit superconductivity, although T_c is drastically lower than with iron. Recently, another superconducting pnictide, SrPtAs, has been discovered, which is the first non-Fe based superconductor with a hexagonal lattice rather than square lattice.⁴ Although $T_c=2.4$ K is lower than those of Fe-based pnictides, it possesses interesting physics associated with its hexagonal crystal structure.

SrPtAs crystallizes in a hexagonal lattice of ZrBeSi type with space group $P6_3/mmc$ (No.194, D_{6h}^4) — the same (non-symmorphic) space group as the hcp structure — with two formula units per primitive cell. As depicted in Fig. 1(a), its structure resembles⁵ that of MgB₂ (with the symmorphic space group $P6/mmm$, No.191, D_{6h}^1), with a double unit cell along the c axis: the boron layers of MgB₂ are replaced by PtAs layers, rotated by 60° in successive layers (responsible for the non-symmorphic nature) and Mg is replaced by Sr. Although the crystal as a whole has inversion symmetry (as do the Sr atoms), the individual PtAs layers lack two-dimensional inversion.

Thus, SrPtAs differs from MgB₂ in two significant ways: (i) it exhibits strong spin-orbit coupling (SOC) at the Pt ions and (ii) the PtAs layers individually break inversion symmetry, exhibiting only C_{3v} (or D_{3h} if z -reflection is included) symmetry. These two properties play an important role in determining the band structure and also affect the superconducting state. Assuming that the superconductivity is largely determined by the two-dimensional PtAs layers, the lack of inversion symmetry in the individual layers (which we call “broken local inversion symmetry”) opens up the

possibility to see the unusual physics associated with non-centrosymmetric superconductors.⁶ With large spin-orbit coupling, nominally s -wave non-centrosymmetric superconductors exhibit spin-singlet and spin-triplet mixing,^{7,8} enhanced spin susceptibilities,^{7,9} enhanced Pauli limiting fields,⁶ non-trivial magnetoelectric effects and Fulde-Ferrell-Larkin-Ovchinnikov(FFLO)-like states in magnetic fields,^{10–16} and Majorana modes.¹⁷ The local inversion symmetry breaking, together with a SOC that is comparable to the c -axis coupling, suggests that SrPtAs will provide an ideal model system to explore related effects in centrosymmetric superconductors.^{18,19}

In this paper we discuss the electronic structure of SrPtAs, including spin-orbit coupling, which was neglected in a previous theoretical study.²⁰ In Sec. II, we describe details of the calculations. The effects of SOC on the bands, the Fermi surface, density of states, and transport properties at the Fermi surface of SrPtAs are presented in Sec. III, along with a tight-binding analysis. Finally, we suggest an enhanced T_c might be possible via doping.

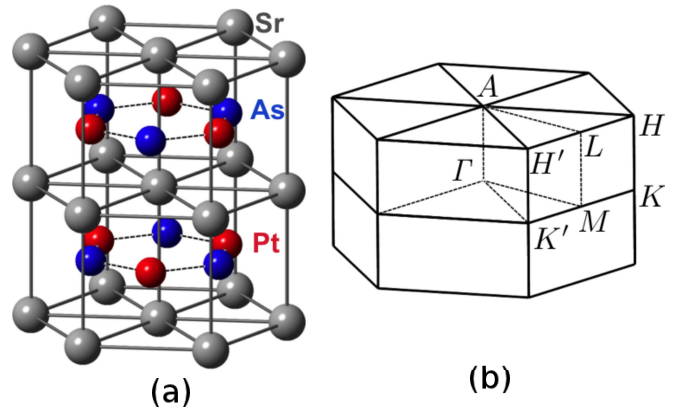


FIG. 1. (a) (Color online) Crystal structure of SrPtAs, where red, blue, and grey spheres denote Pt, As, and Sr atoms, respectively. (b) Brillouin zone of SrPtAs and high symmetry k points.

II. METHOD

First-principles calculations are performed using the full-potential linearized augmented plane wave (FLAPW) method^{21,22} and the local density approximation (LDA) for the exchange-correlation functional of Hedin and Lundqvist.²³ Then, SOC is included by a second variational method.²⁴ Experimental lattice constants, $a = 4.244 \text{ \AA}$ and $c = 8.989 \text{ \AA}$, are used.²⁵ Cutoffs used for wave function and potential representations are 196 eV and 1360 eV, respectively. Muffin-tin radii are 2.6, 2.4, and 2.1 a.u. for Sr, Pt, and As, respectively. Semicore electrons such as Sr 4*p* and As 3*d* are treated as valence electrons, which are explicitly orthogonalized to the core states.²⁶ Brillouin zone summations were done with 90 *k* points in the Monkhorst-Pack scheme,²⁷ while the density of states are obtained by the tetrahedron method.²⁸ Although most of the calculations were performed using LDA, some results were also done with the GGA as well.²⁹ In order to calculate the Fermi velocity and plasma frequency for in-plane and out-of-plane contributions, eigenvalues from self-consistent calculations are fitted by a spline method over the whole Brillouin zone.^{30–32}

III. RESULTS

The band structure of SrPtAs is presented in Fig. 2 along the symmetry lines shown in Fig. 1(b). Plots in the left (right) column are without (with) spin-orbit coupling, and plots in the upper and lower rows are the same but highlighted for As *p* and Pt *d* orbitals, respectively. Our energy bands and Fermi surfaces without SOC agree with those of Ref. [20]. The main band of Sr 5*s* origin is located far above the Fermi level (E_F), consistent with Zintl's scheme³³ that Sr donates electrons to the PtAs layer and behaves almost like an inert Sr^{2+} ion. *Without* SOC, bands on the zone boundary face, the $k_z = \pi/c$ plane ($H - A - L - H$), exhibit four fold degeneracy — two from spin and the other two from two different PtAs layers — as a consequence of the non-symmorphic translations along the *c*-axis, just as for the hcp structure. For the $k_z = 0$ plane ($K - \Gamma - M - K$), there is no such symmetry-dictated degeneracy due to the two equivalent layers, but instead the magnitude of splitting is proportional to the inter-layer coupling. With SOC, the bands change markedly: The four-fold degeneracy on the zone boundary face is reduced to a two fold pseudospin degeneracy due to inversion symmetry, whereas bands along the *A - L* line keeps the fourfold degeneracy as a consequence of time-reversal symmetry.³⁴

In a simple atomic picture, the SOC Hamiltonian is $H_{\text{soc}} = \delta \mathbf{L} \cdot \boldsymbol{\sigma}$, where δ represents the strength of the SOC. Values of the SOC strength derived from the calculations are $\delta_{\text{Pt}} = 0.32 \text{ eV}$ for the Pt *d* orbitals and $\delta_{\text{As}} = 0.23 \text{ eV}$ for As *p* orbitals, which are used in later discussions. The SOC splitting at the A point for Pt d_{xz}, d_{yz} ($d_{xy}, d_{x^2-y^2}$)

orbitals is 0.59 (0.54) eV, whereas for As $p_{x,y}$ the splitting 0.28 eV.

To gain insight into the effect of spin-orbit coupling, we consider a simple tight-binding theory for a single PtAs layer. A single PtAs layer lacks a center of inversion symmetry and therefore allows an anti-symmetric spin-orbit coupling of the form

$$\mathcal{H}_{\text{so}} = \sum_{\mathbf{k}, s, s'} \mathbf{g}_{\mathbf{k}} \cdot \boldsymbol{\sigma}_{ss'} c_{\mathbf{k}s}^\dagger c_{\mathbf{k}s'} \quad (1)$$

exists, where $c_{\mathbf{k}s}^\dagger$ ($c_{\mathbf{k}s}$) creates (annihilates) an electron with momentum \mathbf{k} and pseudo-spin *s*, and $\boldsymbol{\sigma}$ denote the Pauli matrices. Time-reversal symmetry imposes $\mathbf{g}_{\mathbf{k}} = -\mathbf{g}_{-\mathbf{k}}$. Here we find the form of $\mathbf{g}_{\mathbf{k}}$ through a consideration of the coupling between the Pt $d_{x^2-y^2}, d_{xy}$ orbitals and the As p_x, p_y orbitals. These orbitals give rise to the Fermi surfaces with cylindrical topology around the Γ -A line. On the Pt sites, we define states $|d\pm, s\rangle = |d_{x^2-y^2}, s\rangle \pm i|d_{xy}, s\rangle$ and on the As sites we define the states $|p\pm, s\rangle = |p_x, s\rangle \pm i|p_y, s\rangle$ (*s* denotes spin). On a single Pt or As site, the spin-orbit coupling $\mathbf{L} \cdot \mathbf{S}$ has only $L_z S_z$ with non-zero matrix elements in these subspaces. This splits the local four-fold degeneracy into two pairs so that for Pt (As) $|d+, \uparrow\rangle$ and $|d-, \downarrow\rangle$ ($|p+, \uparrow\rangle$ and $|p-, \downarrow\rangle$) form one degenerate pair while $|d+, \downarrow\rangle$ and $|d-, \uparrow\rangle$ ($|p-, \uparrow\rangle$ and $|p+, \downarrow\rangle$) form the other degenerate pair. For both pairs, time-reversal symmetry is responsible for the degeneracy and we can

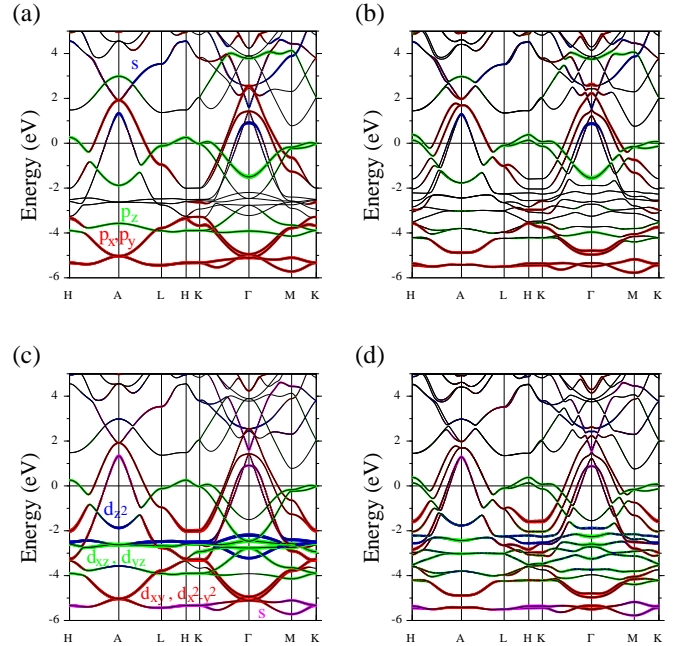


FIG. 2. (Color online) Band structure of SrPtAs (a),(c) without and (b),(d) with spin-orbit coupling. In (a) and (b), As $p_{x,y}$ and p_z orbitals are shown in red and green, respectively, and As *s* in blue. In (c) and (d), Pt ($d_{xy}, d_{x^2-y^2}$), (d_{xz}, d_{yz}), and d_{z^2} orbitals are presented in red, green, and blue, respectively. Contribution from Pt *s* is shown in purple.

label the two degenerate partners of each pair through a pseudo-spin index. We include a spin-independent nearest neighbor hopping between the As and Pt sites. This

yields the following tight binding Hamiltonian in k -space

$$\mathcal{H}_0 = \sum_{\mathbf{k}, s} \Psi_s^\dagger(\mathbf{k}) H_s(\mathbf{k}) \Psi_s(\mathbf{k}), \quad (2)$$

where $\Psi_s(\mathbf{k}) = (c_{\mathbf{k}, d+, s}, c_{\mathbf{k}, d-, s}, c_{\mathbf{k}, p+, s}, c_{\mathbf{k}, p-, s})^T$, s is the spin label ($s = \{\uparrow, \downarrow\}$). For spin up, $H_\uparrow(\mathbf{k})$ is (to get $H_\downarrow(\mathbf{k})$ change the sign of δ_{Pt} and δ_{As})

$$\begin{pmatrix} \epsilon_d + \delta_{Pt} & 0 & t(1 + \nu^* e^{-i\mathbf{k} \cdot \mathbf{T}_3} + \nu e^{i\mathbf{k} \cdot \mathbf{T}_2}) & \tilde{t}(1 + e^{-i\mathbf{k} \cdot \mathbf{T}_3} + e^{i\mathbf{k} \cdot \mathbf{T}_2}) \\ 0 & \epsilon_d - \delta_{Pt} & \tilde{t}(1 + e^{i\mathbf{k} \cdot \mathbf{T}_3} + e^{-i\mathbf{k} \cdot \mathbf{T}_2}) & t(1 + \nu^* e^{i\mathbf{k} \cdot \mathbf{T}_3} + \nu e^{-i\mathbf{k} \cdot \mathbf{T}_2}) \\ \epsilon_p + \delta_{As} & 0 & 0 & 0 \\ 0 & \epsilon_p - \delta_{As} & 0 & 0 \end{pmatrix} \quad (3)$$

where $\nu = e^{i2\pi/3}$, $\mathbf{T}_1 = a(1, 0)$, $\mathbf{T}_2 = a(-1/2, \sqrt{3}/2)$, $\mathbf{T}_3 = a(-1/2, -\sqrt{3}/2)$, t and \tilde{t} are the hopping parameters between the As p and Pt d orbitals, and δ_{Pt} (δ_{As}) is the atomic SOC parameter for Pt d (As p) orbitals. To find an effective Hamiltonian for the Pt d -orbitals, we assume that $|\epsilon_d - \epsilon_p|$ is the largest energy scale and treat all other parameters ($t, \tilde{t}, \delta_{Pt}, \delta_{As}$) as perturbations. This yields the following effective Hamiltonian

$$\mathcal{H}_{Pt} = \sum_{\mathbf{k}, s} \Psi_{Pt, s}^\dagger(\mathbf{k}) H_{Pt, s}(\mathbf{k}) \Psi_{Pt, s}(\mathbf{k}), \quad (4)$$

$$H_{Pt, \uparrow} = \begin{pmatrix} \epsilon_d + \delta_{Pt} + t_1 \sum_i \cos(\mathbf{k} \cdot \mathbf{T}_i) + t_2 \sum_i \sin(\mathbf{k} \cdot \mathbf{T}_i) & t_3 [\cos(\mathbf{k} \cdot \mathbf{T}_1) + \nu \cos(\mathbf{k} \cdot \mathbf{T}_2) + \nu^* \cos(\mathbf{k} \cdot \mathbf{T}_3)] \\ t_3 [\cos(\mathbf{k} \cdot \mathbf{T}_1) + \nu^* \cos(\mathbf{k} \cdot \mathbf{T}_2) + \nu \cos(\mathbf{k} \cdot \mathbf{T}_3)] & \epsilon_d - \delta_{Pt} + t_1 \sum_i \cos(\mathbf{k} \cdot \mathbf{T}_i) - t_2 \sum_i \sin(\mathbf{k} \cdot \mathbf{T}_i) \end{pmatrix} \quad (5)$$

where $t_1 = 2[\tilde{t}^2 + \cos(2\pi/3)t^2]/(\epsilon_d - \epsilon_p)$, $t_2 = -2\sin(2\pi/3)t^2/(\epsilon_d - \epsilon_p)$, and $t_3 = -2t\tilde{t}/(\epsilon_d - \epsilon_p)$, and the sum over i is over the three vectors $\mathbf{T}_1, \mathbf{T}_2$, and \mathbf{T}_3 . The Hamiltonian $H_{Pt, \uparrow}$ yields the dispersions $\epsilon(\mathbf{k}) = t_1(\mathbf{k}) \pm \sqrt{(\delta_{Pt} + t_2(\mathbf{k}))^2 + |t_3(\mathbf{k})|^2}$ where $t_1(\mathbf{k}) = t_1 \sum_i \cos(\mathbf{k} \cdot \mathbf{T}_i)$, $t_2(\mathbf{k}) = t_2 \sum_i \sin(\mathbf{k} \cdot \mathbf{T}_i)$, and $t_3(\mathbf{k}) = t_3 [\cos(\mathbf{k} \cdot \mathbf{T}_1) + \nu \cos(\mathbf{k} \cdot \mathbf{T}_2) + \nu^* \cos(\mathbf{k} \cdot \mathbf{T}_3)]$. The SOC contribution that lifts the four-fold degeneracy into two bands $E_{\mathbf{k}, \pm} = E_{\mathbf{k}} \pm |g(\mathbf{k})|$ at $k_z = \pi/c$ can be found to order $\delta_{Pt}/\sqrt{\delta_{Pt}^2 + |t_2(\mathbf{k})|^2 + |t_3(\mathbf{k})|^2}$ and is given by

$$g(\mathbf{k}) = \hat{z} \frac{t_2 \delta_{Pt}}{\sqrt{\delta_{Pt}^2 + |t_2(\mathbf{k})|^2 + |t_3(\mathbf{k})|^2}} \times [\sin(\mathbf{k} \cdot \mathbf{T}_1) + \sin(\mathbf{k} \cdot \mathbf{T}_2) + \sin(\mathbf{k} \cdot \mathbf{T}_3)] \quad (6)$$

where we have also included the contribution from $H_{Pt, \downarrow}(\mathbf{k})$. Note that this g leads to pseudo-spin interaction in Eq. 1 denoted by σ_z . We emphasize that this σ_z operates on pseudo-spin, not actual spin, the up and down pseudo-spin states are related by time-reversal symmetry (for example, the local states $|d+, \uparrow\rangle$

where $\Psi_{Pt, s}(\mathbf{k}) = (c_{\mathbf{k}, d+, s}, c_{\mathbf{k}, d-, s})^T$, s is the spin label, and

and $|d-, \downarrow\rangle$ form a pseudo-spin pair). The expression for g clearly reveals how the interplay between the atomic SOC (δ_{Pt}) and the broken inversion symmetry ($g(\mathbf{k}) = -g(-\mathbf{k})$) of a single PtAs layer leads to the relevant band SOC. Note that this single-layer band SOC will be of opposite signs for the two inequivalent PtAs layers in the unit cell. Further, the band spin-orbit splitting will have additional contributions from terms of order $\delta_{Pt}/(\epsilon_d - \epsilon_p)$ and $\delta_{As}/(\epsilon_d - \epsilon_p)$ that were neglected in the above derivation. However, these additional contributions do not qualitatively change the results. Similar considerations apply for the other Pt d -orbitals.

The previous paragraph considered a single PtAs layer. To complete the description, the coupling between the two inequivalent layers must be included. For the Pt $d_{x^2-y^2}, d_{xy}$ orbitals considered above, the nearest neighbor inter-layer hopping matrix between $|d+, s\rangle$ states is (the same expression appears for $|d-, s\rangle$ states)

$$\epsilon_c(\mathbf{k}) = t_c \cos(k_z c/2) (1 + e^{-i\mathbf{k} \cdot \mathbf{T}_3} + e^{i\mathbf{k} \cdot \mathbf{T}_2}). \quad (7)$$

Including this inter-layer hopping leads to the following

Hamiltonian

$$\mathcal{H}_{\pm,s} = \sum_{\mathbf{k}} \Psi_{\pm,s}^\dagger(\mathbf{k}) \left\{ [\epsilon_{\pm}(\mathbf{k}) - \mu] \sigma_0 \tau_0 + \mathbf{g}(\mathbf{k}) \cdot \boldsymbol{\sigma} \tau_z \right. \\ \left. + Re[\epsilon_c(\mathbf{k})] \sigma_0 \tau_x + Im[\epsilon_c(\mathbf{k})] \sigma_0 \tau_y \right\} \Psi_{\pm}(\mathbf{k}, s'), \quad (8)$$

where $\Psi_{\pm,s}(\mathbf{k}) = (c_{\pm\mathbf{k}\uparrow 1,s}, c_{\pm\mathbf{k}\downarrow 1,s}, c_{\pm\mathbf{k}\uparrow 2,s}, c_{\pm\mathbf{k}\downarrow 2,s})^T$, 1,2 denote the two inequivalent PtAs layers, σ_i (τ_i) are Pauli matrices that operate on the pseudo-spin (layer) space, $\epsilon_{\pm} = t_1(\mathbf{k}) \pm \sqrt{(t_2(\mathbf{k}))^2 + |t_3(\mathbf{k})|^2}$, and $\mathbf{g}(\mathbf{k})$ is given in Eq. (6) (the τ_z matrix describes the sign change of \mathbf{g} on the two layers). This Hamiltonian can be diagonalized with resulting dispersion relations $\epsilon(\mathbf{k}) = \epsilon_{\pm}(\mathbf{k}) \pm \sqrt{|\epsilon_c(\mathbf{k})|^2 + \mathbf{g}^2(\mathbf{k})}$ and each state is 2-fold degenerate due to time-reversal symmetry (Kramers degeneracy). Note that the tight binding theory described above suggests that eigenstates of S_z are also eigenstates of the single electron Hamiltonian. However, inter-layer coupling terms can lead to additional terms that do not commute with S_z . The band structure suggests that these terms are not large for the states near the Fermi surface.

The SOC found in in Eq. (6) has opposite sign for the different layers as well as for the pseudo-spin direction. This is demonstrated in Fig. 3, where the band structure is resolved by layer and spin for H - L - H' , where L is one of the time-reversal invariant momentum (TRIM) points, and the lines H - L and L - H' are related both by a mirror plane and, and more relevant to the discussion, by a com-

bination of inversion and reciprocal lattice vectors. In Fig. 3, spin up[(a)] and down[(b)] components of the Pt d orbital from the upper PtAs layer are marked in different colors, while components from the other PtAs layers are shown in (c) and (d). As expected from the tight-binding analysis, Figs. 3(a),(d) [and similarly for (b) and (c)] appear the same since they correspond to spatial inversion and time-reversal (opposite spin). Despite the presence of a global inversion center, the locally broken inversion symmetry in PtAs is evident in Fig. 3 where the spin degeneracy is broken in a single layer, for which the consequences are nontrivial.¹⁸ (This result is not surprising or unexpected since in the limit that the coupling between PtAs layers vanishes, i.e., the separation goes to infinity, the single layer result must be recovered.) This spin separation, however, does not result in magnetism because of spin compensation in each layer. These anti-symmetric splittings ($\mathbf{g}(\mathbf{k}) = -\mathbf{g}(-\mathbf{k})$) occur not only at the L point but also at the other TRIM points³⁵ — Γ , A , M , and the A - L line — in the hcp structure.

As expected from the layer structure, anisotropy occurs in the Fermi surfaces, conductivity, and plasma frequency. Two-dimensional cross sections of the Fermi surfaces are shown in Fig. 4, both without [(a)-(d)] and with [(e)-(h)] SOC. Contours in the $k_z = \pi/c$ [(a),(e)] and $k_z = 0$ [(d),(h)] planes clearly exhibit the consequence of the crystal symmetry: hexagonal symmetry around Γ and A and trigonal symmetry around K and H . All sheets exhibit almost two-dimensional cylindrical features except for a small pocket around H . This

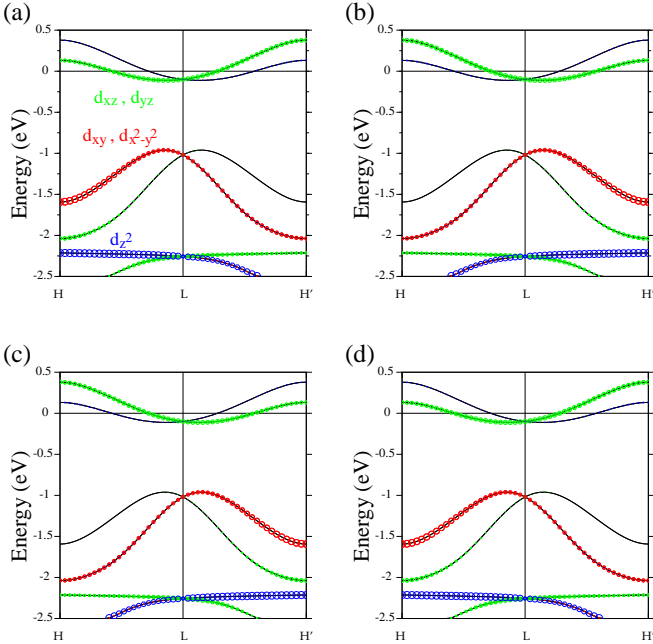


FIG. 3. (Color online) SOC splitting of bands. (a) and (b) [(c) and (d)] show components from Pt 5d orbitals for upper [lower] Pt atoms. Left column[(a) and (c)] is for spin-up components and right[(b) and (d)] is for spin-down components. Radius of circles is proportional to the magnitude of the components.

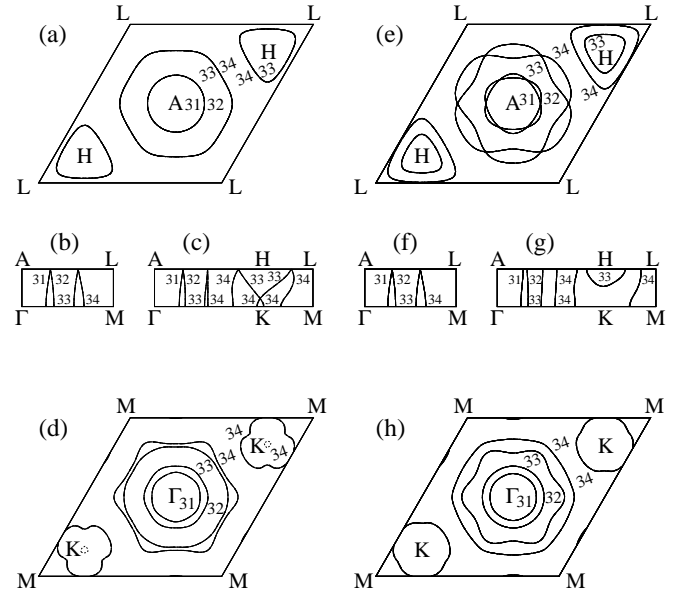


FIG. 4. Cross section of the Fermi surface (a)-(d): without and (e)-(h): with spin-orbit coupling. Cross section along the zone boundary face, $k_z = \pi/c$ [(a),(e)] and at the zone center, $k_z = 0$ [(d),(h)]. (b),(c) are contours along the vertical plane shown with their corner points in the Brillouin zone, where (f),(g) are those with SOC included. Numbers next to Fermi surface sheets indicate band indices.

anisotropy is further exemplified by transport properties which will be discussed later. Moreover, because of the symmetry-dictated degeneracy due to the non-symorphic symmetry, there is no spin-orbit splitting along the time-reversal invariant direction, $A-L$, as seen in Fig. 4(e). Comparing Figs. 4(c) and (g), the SOC appears to make the Fermi surfaces more cylindrical, consequently enhancing the two dimensional character of the Fermi surfaces.

All the Fermi surfaces are hole-like after turning on SOC, in sharp contrast to other pnictide superconductors with two electron-like Fermi surfaces and two hole-like Fermi surfaces.³⁶ Instead of electron-like and hole-like Fermi surfaces, they are distinguished by orbital character. Sheets around the Γ - A line consist of σ orbitals of the PtAs layer, As $p_{x,y}$ and Pt d_{xy,x^2-y^2} , while sheets around the K - H line are from π orbitals, As p_z and Pt $d_{xz,yz}$. Two kinds of Fermi surfaces with different orbital character might give rise to a two energy gap superconductor in SrPtAs.

The anisotropy due to the layered structure is further manifested in the average Fermi velocities and plasma frequencies. Neglecting SOC, the in-plane and out-of-plane Fermi velocities are $\langle v_{x,y}^2 \rangle^{1/2} = 3.72 \times 10^7$ cm/s and $\langle v_z^2 \rangle^{1/2} = 1.02 \times 10^7$ cm/s, respectively, and the plasma frequencies are $\Omega_{x,y} = 5.70$ eV and $\Omega_z = 1.57$ eV. The anisotropy ratio, defined as a ratio of conductivities between in-plane and out-of-plane components, is 13.3, assuming an isotropic scattering rate. With SOC, the anisotropy is enhanced: $\langle v_{x,y}^2 \rangle^{1/2} = 3.76 \times 10^7$ cm/s and $\langle v_z^2 \rangle^{1/2} = 6.78 \times 10^6$ cm/s; $\Omega_{x,y} = 5.57$ eV, $\Omega_z = 1.00$ eV, and the anisotropy ratio increases to a much higher value of 30.8. The decrease of v_z by 33% by SOC is consistent with the enhanced two dimensional character of the Fermi surfaces. Table I summarizes contributions from each Fermi surface. The largest contribution to the density of states at the Fermi level, $N(0)$, comes from the 34th band at around K , which is due to the low velocity at the Fermi surface. The anisotropy ratio is usually much larger than 1 except for the small hole pocket around H .

TABLE I. Fermi surface properties with SOC included for each surface: Density of states, $N(0)$ (states/eV/spin); average velocities, $\langle v_x^2 \rangle^{1/2}$, $\langle v_z^2 \rangle^{1/2}$ (10^7 cm/s); anisotropy ratio, $\langle v_x^2 \rangle / \langle v_z^2 \rangle$; and plasma frequencies, Ω_x , Ω_z (eV). The numbers 31, 32, 33, and 34 represent band indices and Γ and K in the parenthesis represent the locations of the Fermi surface.

	31	32	33(Γ)	34(Γ)	33(K)	34(K)	Total
$N(0)$	0.085	0.107	0.209	0.346	0.267	0.943	1.898
$\langle v_x^2 \rangle^{1/2}$	7.03	6.79	5.92	4.35	1.25	1.68	3.76
$\langle v_z^2 \rangle^{1/2}$	1.03	0.67	0.47	1.04	1.37	0.41	0.678
$\langle v_x^2 \rangle / \langle v_z^2 \rangle$	46.9	103	159	17.3	0.83	16.9	30.8
Ω_x	2.20	2.39	2.91	2.74	0.69	1.75	5.57
Ω_z	0.32	0.24	0.23	0.66	0.76	0.43	1.00

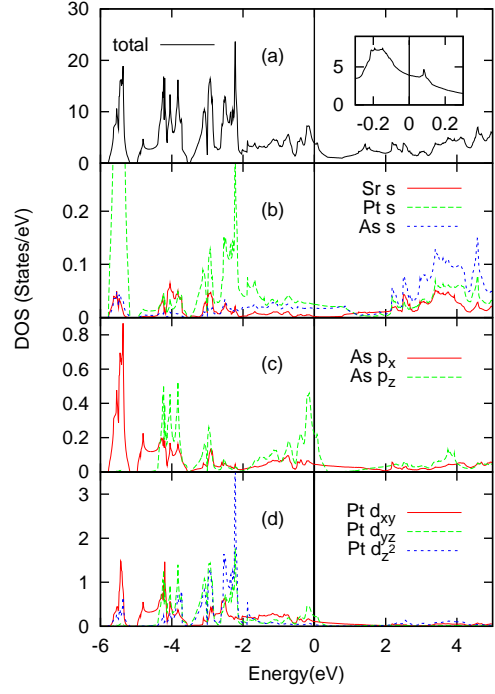


FIG. 5. (Color online) Density of states (DOS) of SrPtAs: (a) total DOS, (b) s orbitals, (c) As p orbitals, and (d) Pt d orbitals.

The total density of states (DOS) and orbital decomposed partial DOS are presented in Fig. 5. The states around E_F arise mainly from As p and Pt d . The non-bonding Pt d_{z^2} bands are located at around -2.2 eV, and because they hybridize little with other orbitals, they give rise to a peak in the DOS. In contrast, π -bonding orbitals such as As p_z and Pt $d_{xz,yz}$ are located around the Fermi level with a wide band width. In particular, the van Hove singularity (vHS) coming from a saddle point near K just above E_F (inset of Fig. 5(a)) exhibits two dimensional character since a 2D vHS gives rise to a singularity in the DOS while a 3D vHS gives only a discontinuity in slope. Raising E_F to vHS, which might be realized by electron doping via Sr layers, could potentially increase T_c : Assuming rigid bands, we estimate that electron doping by roughly 25% will lift E_F to the vHS, enhancing the DOS at the Fermi level by 6%. Further, using a weak-coupling form for T_c ($T_c = 1.14 T_D e^{-1/N(0)V}$), assuming that the pairing potential V does not change by electron doping, and assuming Debye temperature of $T_D = 229$ K,³⁷ we estimate that T_c could be enhanced to as high as 3.8 K by electron doping.

Applying hydrostatic pressure could also raise the DOS and could, as often happens, enhance T_c . Rh is a candidate to supply a chemical pressure to SrPtAs since it has a similar electronegativity as Pt but a smaller ionic radius. However, the crystal structure is sensitive to the constituent atoms; for example, SrPtSb where As is replaced by Sb has an AlB₂-type structure, while YPtAs, where Sr is replaced by Y with more electrons, has a

hexagonal structure with four slightly puckered PtAs layers in a unit cell.⁵

Finally we consider the possibility of simple collinear magnetic solutions. The antiferromagnetic (AFM) phase, where the moments in a PtAs layer are aligned, by antiparallel to those in adjacent layers, is favored by 0.23 meV (0.49 meV in GGA) per formula unit, than the non-magnetic phase; the ferromagnetic orientation converged to the non-magnetic solution. Magnetic moments are given in Table II. While the energy differences and calculated moments are too small to make definitive statements regarding magnetic phases in SrPtAs, the material appears to be near a magnetic instability.

IV. SUMMARY

First-principles calculations of the electronic structure of SrPtAs have been presented with SOC fully taken into account. The role of SOC on the electronic structure is manifested in the energy bands and Fermi surfaces. The important physics originates from two factors: strong SOC in Pt atoms and locally broken inversion symmetry in PtAs layers. We have constructed a tight-binding Hamiltonian based on the self-consistent electronic structure that provides insight into the SOC. Sheets of the Fermi surface are spatially well separated in the Brillouin zone: cylindrical Fermi surfaces with σ -character at the zone center (around Γ -A) and two Fermi sur-

faces, *i.e.*, a pocket and a cylinder, with π -character at the zone corner (around K -H). All the Fermi surfaces are hole-like which distinguishes this material from other pnictide superconductors. The transport properties are highly anisotropic between x, y - and z - directions. Rh is suggested for a positive pressure effect to increase T_C . Furthermore, the van Hove singularity is shown in the DOS above E_F . Assuming rigidity of bands, we predict that T_C increases up 3.4 K with 25% doping, which may be achieved by chemical doping in place of the Sr atom.

ACKNOWLEDGMENTS

SJY and SHR are indebted to Hosub Jin for fruitful discussions. SJY acknowledges the sabbatical research Grant by Gyeongsang National University. SHR and AJF are supported by the Department of Energy (DE-FG02-88ER45382). DFA is supported by NSF grant DMR-0906655. MW is supported by NSF DMR-1105839.

TABLE II. Spin μ_s and orbital μ_l magnetic moments and total magnetic moment μ_t in unit of μ_B .

	μ_s	μ_l	μ_t
Pt	0.014	0.064	0.078
As	0.006	-0.027	-0.021

- ¹ Y. Kamihara, T. Watanabe, M. Hirano, and H. Hosono, J. Am. Chem. Soc. **130**, 3296 (2008).
- ² C. Wang, L. Li, S. Chi, Z. Zhu, Z. Ren, Y. Li, Y. Wang, X. Lin, Y. Luo, S. Jiang, et al., Europhys. Lett. **83**, 67006 (2008).
- ³ I. Mazin and J. Schmalian, Physica C **469**, 614 (2009).
- ⁴ Y. Nishikubo, K. Kudo, and M. Nohara, J. Phys. Soc. Jpn. **80**, 055002 (2011).
- ⁵ R.-D. Hoffmann and R. Pöttgen, Z. Kristallogra. **216**, 127 (2001).
- ⁶ P. A. Frigeri, D. F. Agterberg, A. Koga, and M. Sigrist, Phys. Rev. Lett. **92**, 097001 (2004).
- ⁷ L. Gor'kov and E. Rashba, Phys. Rev. Lett. **87**, 037004 (2001).
- ⁸ H. Yuan, D. Agterberg, N. Hayashi, P. Badica, D. Vandervelde, K. Togano, M. Sigrist, and M. Salamon, Phys. Rev. Lett. **97**, 017006 (2006).
- ⁹ P. A. Frigeri, D. Agterberg, and M. Sigrist, New J. Phys. **6**, 115 (2004).
- ¹⁰ V. Barzykin and L. Gor'kov, Phys. Rev. Lett. **89**, 227002 (2002).
- ¹¹ D. F. Agterberg, Physica C **387**, 13 (2003).
- ¹² R. P. Kaur, D. F. Agterberg, and M. Sigrist, Phys. Rev. Lett. **94**, 137002 (2005).
- ¹³ K. V. Samokhin, Phys. Rev. B **78**, 224520 (2008).
- ¹⁴ V. M. Edelstein, J. Phys.: Condens. Matter **8**, 339 (1996).
- ¹⁵ S. K. Yip, Phys. Rev. B **65**, 144508 (2002).
- ¹⁶ S. Fujimoto, Phys. Rev. B **72**, 024515 (2005).
- ¹⁷ M. Sato and S. Fujimoto, Phys. Rev. B **79**, 094504 (2009).
- ¹⁸ S. J. Youn, M. H. Fischer, S. H. Rhim, M. Sigrist, and D. F. Agterberg, e-print arXiv:cond-mat/1111.5058 (2011).
- ¹⁹ M. H. Fischer, F. Loder, and M. Sigrist, Phys. Rev. B **84**, 184533 (2011).
- ²⁰ I. Shein and A. Ivanovskii, Physica C **471**, 594 (2011).
- ²¹ E. Wimmer, H. Krakauer, M. Weinert, and A. J. Freeman, Phys. Rev. B **24**, 864 (1981).
- ²² M. Weinert, E. Wimmer, and A. J. Freeman, Phys. Rev. B **26**, 4571 (1982), and references there in.
- ²³ L. Hedin and B. I. Lundqvist, J. Phys. C. **4**, 2064 (1971).
- ²⁴ A. H. MacDonald, W. E. Pickett, and D. D. Koelling, J. Phys. C **13**, 2675 (1980).
- ²⁵ G. Wenski and A. Mewis, Z. Anorg. Allg. Chem. **535**, 110 (1986).
- ²⁶ M. Weinert, G. Schneider, R. Podloucky, and J. Redinger, J. Phys.: Cond. Matt. **21**, 084201 (2009).
- ²⁷ H. J. Monkhorst and J. D. Pack, Phys. Rev. B **13**, 5188 (1976).
- ²⁸ P. E. Blöchl, O. Jepsen, and O. K. Andersen, Phys. Rev. B **49**, 16223 (1994).
- ²⁹ J. P. Perdew, K. Burke, and M. Ernzerhof, Phys. Rev. Lett. **77**, 3865 (1996).
- ³⁰ D. D. Koelling and J. H. Wood, J. Comp. Phys. **67**, 253 (1986).
- ³¹ W. E. Pickett, H. Krakauer, and P. B. Allen, Phys. Rev. B **38**, 2721 (1988).

- ³² G. K. H. Madsen and D. J. Singh, J. Comput. Phys. Comm. **175**, 67 (2006).
- ³³ H. Schäfer, Ann. Rev. Mater. Sci. **15**, 1 (1985).
- ³⁴ L. F. Mattheiss, Phys. Rev. **151**, 450 (1966).
- ³⁵ L. Fu, C. L. Kane, and E. J. Mele, Phys. Rev. Lett. **98**, 106803 (2007).
- ³⁶ D. J. Singh and M.-H. Du, Phys. Rev. Lett. **100**, 237003 (2008).
- ³⁷ K. Kudo (2011), private communication.